Naval Research Laboratory
Stennis Space Center, MS 39529-5004

NRL/MR/7181--94-7533

FInite Difference Ocean Acoustic Model Users Guide

R. A. ZINGARELLI

Acoustics, Tactics, and Simulation Branch
Center for Environmental Acoustics

December 23, 1994

REPORT DOCUMENTATION PAGE

Form Approved
OBM No. 0704-0188

1. Agency Use Only *(Leave blank).*

2. Report Date.
December 23, 1994

3. Report Type and Dates Covered.
Final

4. Title and Subtitle.
FInite Difference Ocean Acoustic Model Users Guide

5. Funding Numbers.
Program Element No. 0602435N
Project No.
Task No.
Accession No.
Work Unit No. 71-5013-04

6. Author(s).
R. A. Zingarelli

7. Performing Organization Name(s) and Address(es).
Naval Research Laboratory
Center for Environmental Acoustics
Stennis Space Center, MS 39529-5004

8. Performing Organization Report Number.
NRL/MR/7181--94-7533

9. Sponsoring/Monitoring Agency Name(s) and Address(es).
Office of Naval Research
800 N. Quincy St.
Arlington, VA 22217-5000

10. Sponsoring/Monitoring Agency Report Number.

11. Supplementary Notes.

12a. Distribution/Availability Statement.
Approved for public release; distribution is unlimited.

12b. Distribution Code.

13. Abstract *(Maximum 200 words).*

The computer program FIDO (FInite Difference Ocean acoustic model) computes the real acoustic pressure via a finite-difference approximation to the undamped wave equation, with attenuation implemented by the insertion of an additional radiation condition term in sediment regions of the computation grid. The program is implemented in FORTRAN and is well suited to most supercomputer architectures. Both time-domain and continuous-wave versions are described. Input file formats are given along with two sample input files. Test cast solutions for standard benchmarks and other problems are presented and compared to analytic and coupled-mode solutions.

14. Subject Terms.
finite difference, time domain

15. Number of Pages.
14

16. Price Code.

17. Security Classification	**18. Security Classification of Report.**	**19. Security Classification of This Page.**	**20. Limitation of Abstract. of Abstract.**
Unclassified	Unclassified	Unclassified	SAR

NSN 7540-01-280-5500

Standard Form 298 (Rev. 2-89)
Prescribed by ANSI Std. Z39-18
298-102

FINITE DIFFERENCE OCEAN ACOUSTIC MODEL USERS GUIDE

INTRODUCTION

Direct assault of the wave equation in an underwater environment via the finite difference (FD) method has been tried from time to time with varying degrees of success. The FD method has several advantages over other methods commonly used to solve underwater acoustics problems. Chief among these is that the wave equation itself is being solved, rather than a more tractable approximation of the equation. Another advantage is that very complicated boundary shapes and conditions require almost no extra theoretical or computational effort. Finally, the simplicity of the theory and its implementation in a program lends credibility and confidence to the results generated. Disadvantages of the FD method include (in usual order of importance) excessive computation times, instabilities and discretization errors in the solution, problems in absorptive media, and problems at radiating boundaries. Until recently, these disadvantages have made the FD method in underwater acoustics an interesting technique, occasionally implemented at short ranges and low frequencies for specific research goals [1,2]. Generally, it has been of little practical importance to acoustic propagation over realistic ocean environments. However, the FD method has one additional feature that meshes with recent advances in computing technology and now makes it useful; it is inherently parallel at all scales.

FINITE DIFFERENCE REPRESENTATION OF THE WAVE EQUATION

The wave equation describing the real acoustic pressure Ψ is the following:

$$\nabla^2\psi = \frac{1}{c^2}\frac{\partial^2\psi}{\partial t^2}\,, \qquad (1)$$

where c is the local sound speed. Converting from the continuum to an FD formulation and invoking axial symmetry to reduce the problem to two dimensions transforms Eq. (1) into:

$$U_{i;j}^{n+1} = 2U_{i;j}^{n} - U_{i;j}^{n-1} + c^2\frac{\Delta t^2}{\Delta x^2}\left[U_{i+1;j}^{n} + U_{i-1;j}^{n} + U_{i;j+1}^{n}\ U_{i;j-1}^{n} - 4U_{i+1;j}^{n}\right], \qquad (2)$$

where i and j are the indices in range and depth respectively, n is the index in time, and $U(r,z) \equiv \Psi(r,z,\phi)/r$.

Boundaries and their conditions are shown in Fig. 1. At the left edge, axial symmetry is implemented by reflecting the field about the central axis, i.e., $U(-\Delta x,z) = U(\Delta x,z)$. At the top surface, a pressure release boundary is enforced by setting $U(r,0) = 0$. At the right and bottom edges, radiation conditions are implemented:

$$\frac{dU}{dt} = -c\frac{dU}{dx}\,, \qquad (3)$$

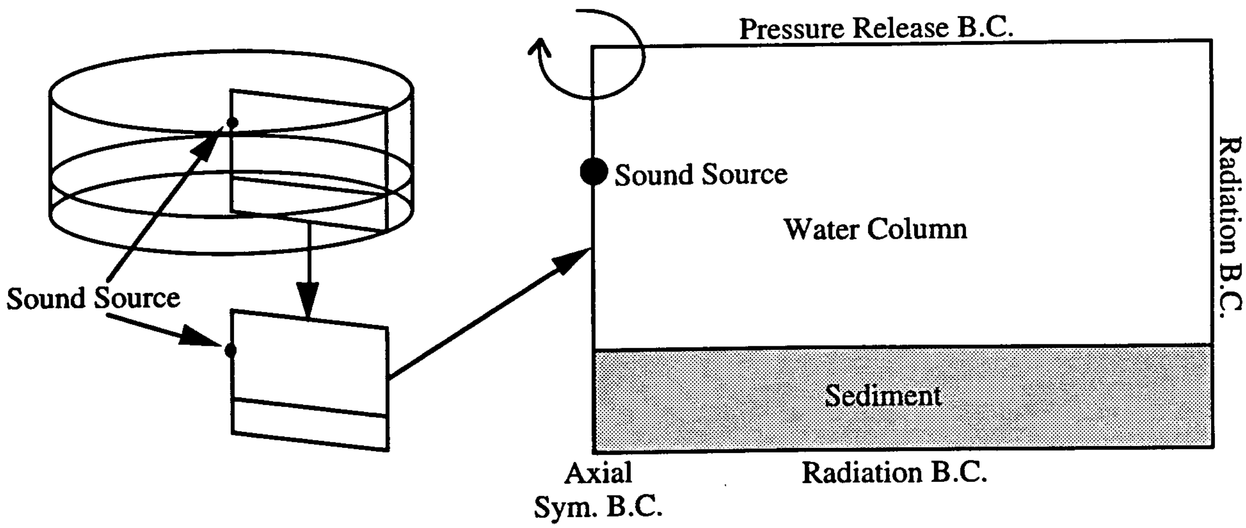

Fig. 1 — Geometry and boundaries used by FIDO and the relationship between three-dimensional axially symmetric problem and two-dimensional solution grid.

where x can either be in range or depth. Without having information one spacing outside of the computation grid, the first derivative dU/dx cannot be directly calculated at the boundary to any acceptable precision. However, both the first and second derivatives are directly available at the point one step inside of the grid. By using a Taylor expansion from this point, an acceptable approximation of the first derivative at the grid boundary is possible:

$$\frac{dU(x)}{dx} \approx \frac{dU(x-\Delta x)}{dx} + \frac{d^2U(x-\Delta x)}{dx^2}\Delta x \,. \tag{4}$$

Transformed into FD representations and combined, Eqs. (3) and (4) become:

$$U_i^{n+1} = U_i^n - c\frac{\Delta t}{\Delta x}\left[\frac{3}{2}U_i^n - 2U_{i-1}^n + \frac{1}{2}U_{i-2}^n\right]. \tag{5}$$

Attenuation is handled in a fashion related to boundary radiation. At grid points in an attenuating medium, the solution is augmented by an absorptive part, so that Eq. (4) becomes:

$$U_{i;j}^{n+1} = (1-\gamma)\,U_{wave} + \gamma\,U_{radiation}\,, \tag{6}$$

where U_{wave} is the unattenuated wave solution from Eq. (2), $U_{radiation}$ is a simplified first-order version of the radiation condition from Eqs. (3) and (4), and the mixing ratio γ is related to the usual attenuation coefficient $\beta(\mathrm{dB}/\lambda)$ by: $\log_{10}(1-\gamma) = (\beta\Delta x)/(-20\lambda\eta)$, where η is the span of elements the first derivative is taken from, i.e., 1 if $dU/dx \approx (U(x) - U(x-\Delta x))/\Delta x$, or 2 if $dU/dx \approx (U(x+\Delta x) - U(x-\Delta x))/\Delta x$. Typically γ is small, on the order of 10^{-3}. The derivative used in calculating the attenuation is user-selectable but not of great importance. The former approximation seems to give slightly better results overall, but the latter expression occasionally gives better results deep in sediment layers.

Three additional boundary conditions are allowed in the FInite Difference Ocean acoustic model (FIDO): pressure release "bubbles" are inserted after the body of the computations have been performed at each time step by setting the field to zero at user-specified grid points; hard surface "rock layers" are similarly inserted by copying the field values just outside of a surface into the boundary elements, thus forcing the first derivative across the interface to zero; and hard surface grid point "rocks" that are simulated by recalculating the four neighboring grid points with the first derivative set to zero in each direction.

The von Neuman analysis indicates that Eq. (2) will be stable for time steps smaller than $\Delta x/(\sqrt{2}\ c)$. In practice, this must be reduced to $\Delta x/(2c)$ to ensure stability. Values for Δx on the order of $\lambda/5$ give recognizable transmission loss (TL) curves when solving benchmark problems, but $\lambda/10$ is much better; maximum accuracy seems to be reached by $\lambda/30$. Similar analysis shows that Eq. (5) is at the threshold of stability for this value of Δt but can never be stable. Fortunately, the extra margin of stability on the main grid from a slightly smaller time step, truncation of the solution to 32-bit precision, and the fact that the solution is radiating away from the main grid at these points, all combine to give an acceptably stable solution. Because Eq. (5) is also used for absorption, the solution can become unstable for sediment attenuation values significantly greater than 1 dB/λ; for attenuations below this value the errors are simply damped out.

In order to simulate a continuous-wave (CW) problem, a sinusoidal source is placed in the grid (usually at the left edge in Fig. 1, in order to give axial symmetry), and the resulting energy is allowed to propagate throughout the grid until a steady state is reached. The time required for this to happen is approximately twice the time for sound to propagate from one end of the waveguide to the other. After simulating out to this time, peak values at each grid point of interest are sampled over the last 10 periods of the run. These are then used to generate TL curves and/or full-field plots. Simulating a time-domain problem is even more straightforward. Some arbitrary set of source functions is fed into the grid and allowed to propagate to regions of interest where it is sampled as a time series (TS). Multiple widely spaced pulses can be simultaneously propagated on the same grid, further increasing computational efficiency.

COMPUTATIONAL DETAILS

The array containing the field is dimensioned as illustrated in Fig. 2. The field is held at all ranges and depths for three time steps: one past, the present step, and the future step being computed. After the next time step is computed, a set of integer pointers is rearranged so that the frame holding the "future" field values becomes the "present" frame, the old "present" becomes the "past," and the old "past" frame is set to be overwritten by the new "future." This pointer method is much more efficient than actually moving the field values to appropriate memory locations, particularly on vector supercomputers where bulk memory moves can be as time consuming as floating point operations.

To date, FIDO has been implemented on three different supercomputer architectures with four different computational schemes. On a Thinking Machine Corporation CM-200, an early version was implemented by assigning each grid point and its associated time slices and weighting coefficients to each virtual processor. At each step in the computation, the processors would poll their nearest neighbors and compute new values. On the Cray Research Y-MP/8 vector/parallel machine, the innermost loop of the grid computation (over range) was vectorized, and the depth loop was parallelized. As before, the time-step loop was computed sequentially, which is an inherent, if distant, limitation to parallelization in this model. On a Silicon Graphics Challenge L 8xR4400/150 (8 150 MHz R4400 processors), two parallelization schemes were tried: over range and executing the depth loop

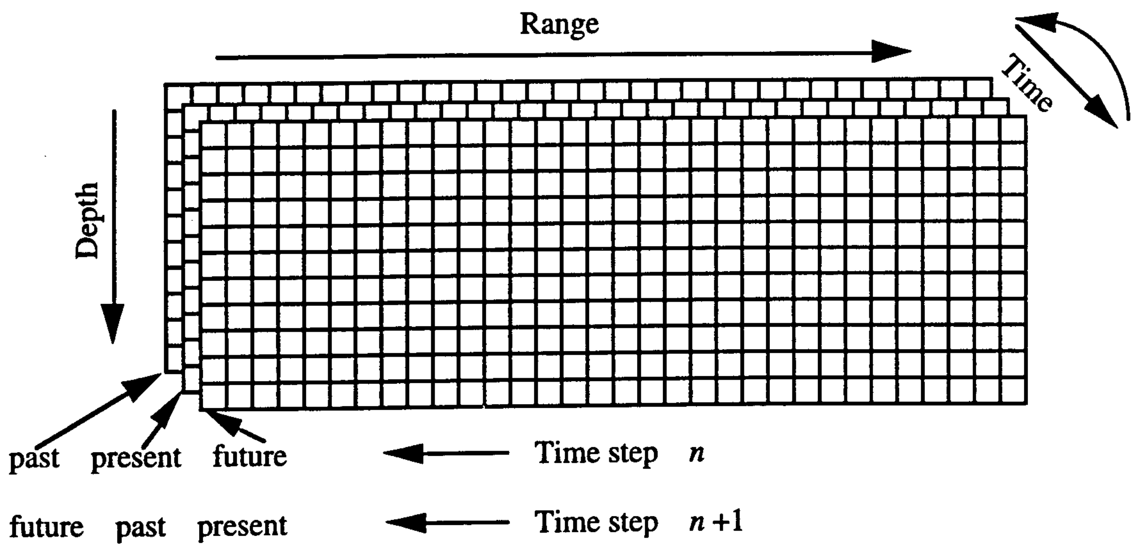

Fig. 2 — Organization of field array and time-step pointers. By rearranging the past, present, and future pointers, old results are overwritten and massive memory transfers are avoided.

sequentially; and over depth, executing many inner range loops sequentially. The latter method has significantly lowered overhead and executes about three times faster. Runtimes for the Acoustical Society of America (ASA) penetrable lossy wedge [3] benchmark on a 400- by 4000-m grid using a 4-m step size are 5 and 37 s, respectively, for a Y-MP/8 and a Challenge L 8xR4400/150. These execution speeds are comparable to those of older parabolic equation codes such as FEPE and PAREQ [4], which though more economical to execute on SISD computers, cannot make efficient use of supercomputers.

THE CODES AND INPUT FILES

The overall structure of FIDO is as follows:

```
get input data;
precalculate source parameters;
precalculate weights for grid computations;
clear field arrays;
loop over time
  update main body of grid using Eqs. (2) and (6);
  update edge boundaries of grid using Eq. (5);
  if used, then insert bubbles and rocks;
  update source point(s);
  if near end of run, sample grid;
end time loop;
write results;
exit.
```

Some array initialization is performed in a separate input routine, but the bulk of the computations and memory are held in the main routine. Although this is generally a poor programming practice, it was done in this case to minimize memory requirements and time spent passing data. Because different computer manufacturers implement the FORTRAN standard for parameter passing in a variety of ways, it is best to sidestep the problem and simply avoid passing these large arrays altogether.

Because the input and output requirements for CW and time-domain solutions are so different, two versions of FIDO have been written. One (FIDO) steps through enough time that a CW solution is approximated, then samples and writes out TL curves and the full field to various files. The other version (FIDOP) injects pulses into the grid centered at time = 0 and runs long enough for the pulse to interact with the environment and propagate to all receivers specified by the user. It should be noted that the computational kernels of the two versions are *identical*, and they could be combined into a single code with appropriate input and output routines, if the memory and data passing requirements discussed previously were not so severe.

The input file format generally follows that used by FEPE [5], with a few exceptions. For FIDO (CW version), the file name is fido.in, and the format is the following:

```
TITLE
FREQ, ZS, [-]ZR
[ZR1, . . .]
Rmax, dR, ndR
Zmax, dZ, ndZ
c0, iDeriv
unused, leftEdge, iAxSym
(bathymetry block)
(profile block)
[Rp
(profile block)
[Rp]]
```

Bracketed items are optional. The bathymetry block has the format:

```
RD   D
.    .
RD   D
-1   -1
```

where –1's indicate the end of the bathymetry block. The profile blocks have the format:

```
Z    CW
.    .
Z    CW
```

```
-1   -1
Z    CB
.    .
Z    CB
-1   -1
Z    rhoB
.    .
Z    rhoB
-1   -1
Z    ATTEN
.    .
Z    ATTEN
-1   -1
```

where the –1's indicate the end of the subblocks. The items are as follows:

TITLE	alphanumeric tag for file describing its contents.
FREQ	source frequency (Hz).
ZS	source depth (m).
ZR	receiver depth (m). If negative, then it is the number of receiver depths to be read from the next line.
Rmax	maximum range in computation (m).
dR	range step size (m) (same as dZ).
ndR	range step increment between full-field output points.
Zmax	maximum depth in computation (m).
dZ	depth step size (m) (same as dR).
ndZ	depth step increment between full-field output points.
c0	reference sound speed used to compute time step. Usually best set to the maximum sound speed in the environment.
iDeriv	switch to select grid points used in determining derivative used in calculating attenuation: 1 = use $U(i)$ and $U(i \pm 1)$ at the ith point. 2 = use $U(i+1)$ and $U(i-1)$ at the ith point.

leftEdge switch to select left edge boundary condition:

1 = symmetry condition $\frac{dU}{dr} = 0$ imposed at left boundary by setting $U(-\Delta r,z) = U(\Delta r,z)$.

2 = absorbing B.C. from Eq. (5) used.

iAxSym switch for point (1) or line (2) source when computing TL curves.

RD range of a bathymetry point (m).

D depth of a bathymetry point (m).

Z depth of a profile point (m).

CW sound speed in the water (m/s).

CB sound speed in the bottom (m/s).

rhoB density in the bottom (g/cm^3) (currently unused).

ATTEN attenuation in the bottom (dB/λ).

RP range to next profile (m) (optional, if at end of last profile).

unused unused item, included in file for compatibility with FEPE.

The input file for FIDOP (fidop.in) is similar and identical after the receiver position specifications:

```
TITLE
freqC, sigmaF, nFreq, Zs, nReceivers
Zreceiver1 [Zreceiver2 . . .]
Rreceiver1 [Rreceiver2 . . .]
```

where the items are as follows:

freqC center frequency of a Gaussian pulse (Hz).

sigmaF width of the pulse (Hz).

nFreq number of frequencies to be summed to form the pulse.

nReceivers number of TS receivers for problem.

Zreceiver depth(s) of receiver(s) (m).

Rreceivers range(s) of receiver(s) (m).

Because attenuation is translated from the input dB/λ into fraction of the energy lost at each grid step, the attenuation parameter γ from Eq. (6) is calculated using the wavelength as the center frequency of the pulse.

An additional file, fido.bc, contains rocks and bubbles as discussed in the Introduction. The format for this file is the following:

```
range depth   key
[repeat as needed],
```

where range and depth are the position of the object in meters, and key is an integer specifying the type of boundary to be applied. If key is –1, then a pressure release boundary is used. If key is in the range 1 to 8, then the first derivative will be set to zero in the direction shown in Fig. 3. If key is set to any other positive value, then the field values at the four adjacent grid points are recalculated with the first derivative set to zero in each direction. In simulating hard surfaces, keys 1 through 8 should be used whenever possible, since no recalculation is needed to implement this type of simulated bouldery. If no additional boundary condition points are being used in a calculation, then the additional boundary condition file should be renamed or deleted entirely, since its presence in a users directory forces FIDO to search through the grid for these special points at each time step. This search procedure can inflict approximately a 20% runtime penalty on the program's execution.

8	1	2
7	cell being calculated	3
6	5	4

Fig. 3 — Key code giving direction across which first derivative will be taken in calculating field value in central cell.

EXAMPLES

The ASA penetrable lossy wedge problem is described by the FIDO input file in Table 1, and TL curves from this computation, overlaid with results of a two-way coupled mode calculation produced by the code COUPLE [3,6], are shown in Fig. 4b. An additional complication, a Cantor dust screen of bubbles halfway out in the waveguide, is shown in Fig. 5. The resulting TL curve generated by FIDO for the shallow receiver depth, corresponding to Fig. 4a, is shown in Fig 6. By reducing the range step to 2 m, using the line source and absorbing left boundary options, inserting a pressure-release boundary layer along the bottom, and moving the source to a 4-m range, the ASA ideal wedge benchmark problem was attempted; the results of this calculation, along with an analytic solution [7] at close range, are shown in Fig. 7. The environment for problem 2a from the Reverberation and Scattering Workshop [8] is shown in Fig. 8 and given in the form of a FIDOP input file in Table 2. The resulting time series is shown in Fig. 9.

Overall, the FIDO solutions for the ASA wedge problems are close to the reference solutions in magnitude and form. The agreement with the analytic solution for the ideal wedge case indicates that the undamped wave equation solution in Eq. (2), scattering from pressure release surfaces and boundary absorption using Eq. (5), have been combined to produce reliable results. The chief discrepancies in the TL curves for the penetrable wedge problem seem to occur at ranges where modes drop out of the field. There, COUPLE can treat the problem in an exact manner, but the approximations inherent in FIDO tend to smear the solution. Instability in the sediment attenuation method may also contribute to these difficulties. In the case of the time domain problem, the FIDO and COUPLE time series for the reflected pulse are identical for the first two cycles, indicating that the propagation and scattering methods of the two models are equivalent. Discrepancies occurring after this are due to differences in the treatment of attenuation by the two codes. These problems may result from the unstable attenuation condition (as in the CW case), or from the fact that FIDO ignores frequency dependence in calculating sediment absorption of pulses.

Table 1 — FIDO input file, fido.in, for ASA penetrable wedge benchmark

WEDGE BENCHMARK			
25.0	100.0	−2.1	FREQ ZS nTL
30.0	150.0		Zreceiver(s)
4000.0	2.0	10	RMAX DR NDR
1000.0	2.0	10	ZMAX DZ NDZ
1700.0	1		C0 iDeriv
0 1 1			(unused), axial sym left B.C., point source
0.0	200.0		BATHYMETRY
4000.0	0.0		
−1 −1			
0.0	1500.0		Z CW
−1 −1			
0.0	1700.0		Z CB
−1 −1			
0.0	1.5		Z RHOB
−1 −1			
0.0	0.5		Z ATTNP
1000.0	0.5		
−1 −1			

Table 2 — FIDOP input file, fidop.in, for Reverberation and Scattering Workshop, Case 2A

REVERBERATION AND SCATTERING WORKSHOP, CASE 2A					
30.0	10.0	256	50.0	2	freqC, sigmaF, nFreq, ZS, nReceivers
45.0	45.0				Zreceiver(s)
5.0	3000.0				Rreceiver(s)
4000.0	2.0	10			RMAX DR NDR
1000.0	2.0	10			ZMAX DZ NDZ
1800.0	1				C0 iDeriv
0 2 1					(unused), absorbing left B.C., point source
0.0	150.0				BATHYMETRY
2999.0	150.0				
3000.0	50.0				
3120.0	50.0				
3121.0	150.0				
4000.0	150.0				
−1 −1					
0.0	1500.0				Z CW
−1 −1					
0.0	1800.0				Z CB
−1 −1					
0.0	1.5				Z RHOB
−1 −1					
0.0	0.5				Z ATTNP
400.0	0.5				
−1 −1					

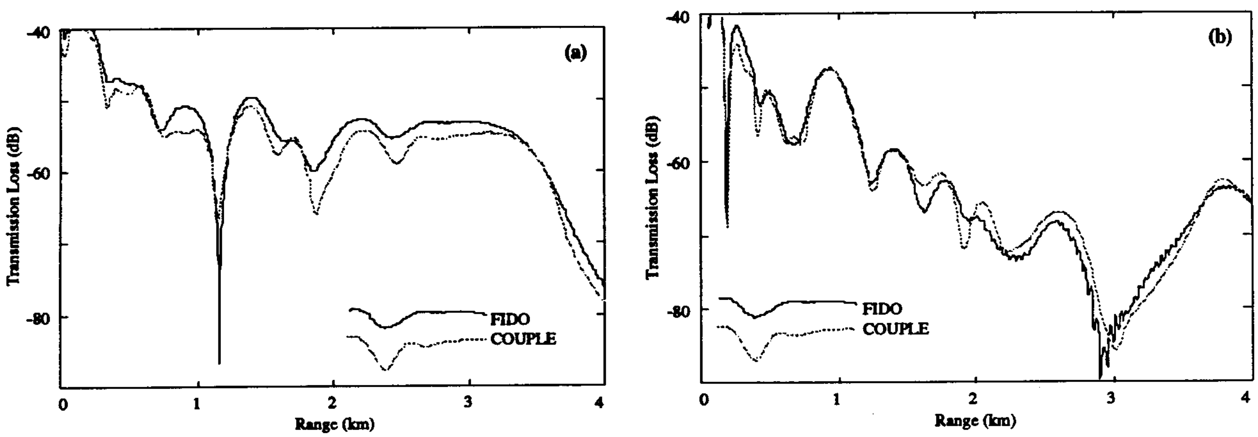

Fig. 4 — ASA penetrable loss wedge benchmark problem solutions for FIDO and COUPLE. Receiver depths are (a) 30 m and (b) 150 m.

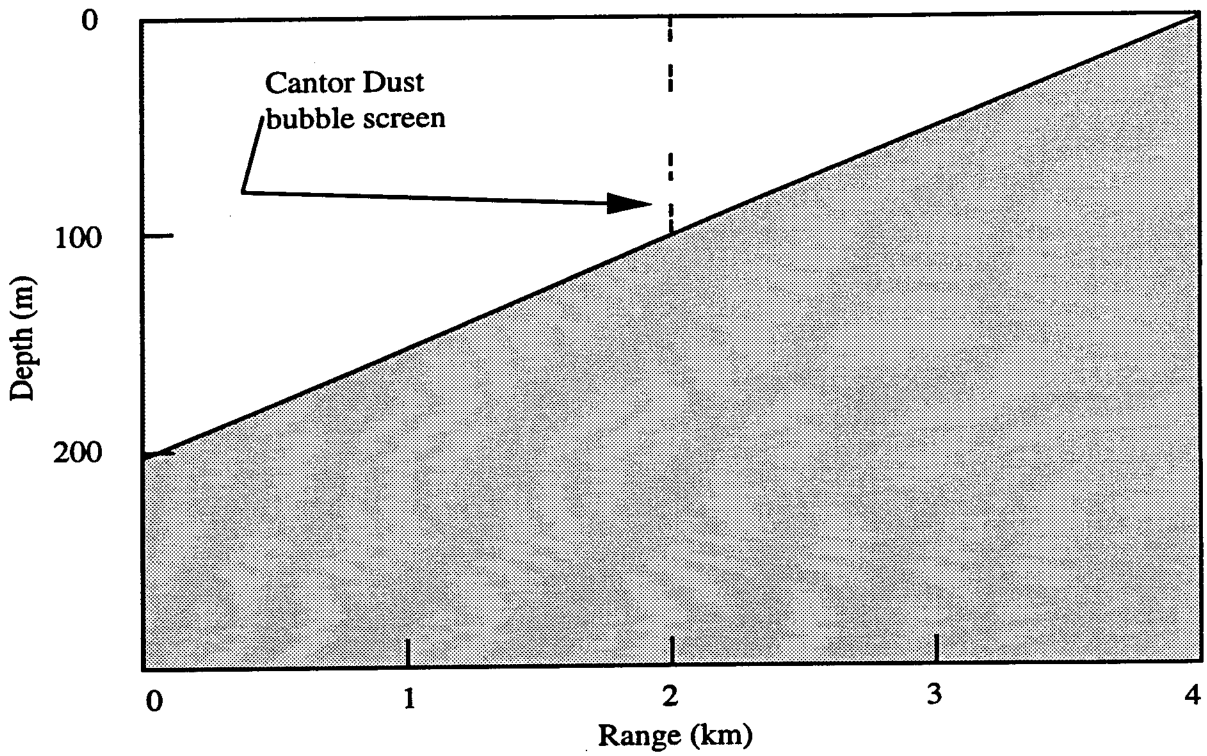

Fig. 5 — ASA benchmark penetrable lossy wedge problem modified by addition of a simple fractal bubble screen. Bandwidth of the fractal is bounded by water column depth (100 m) and grid size (2 m).

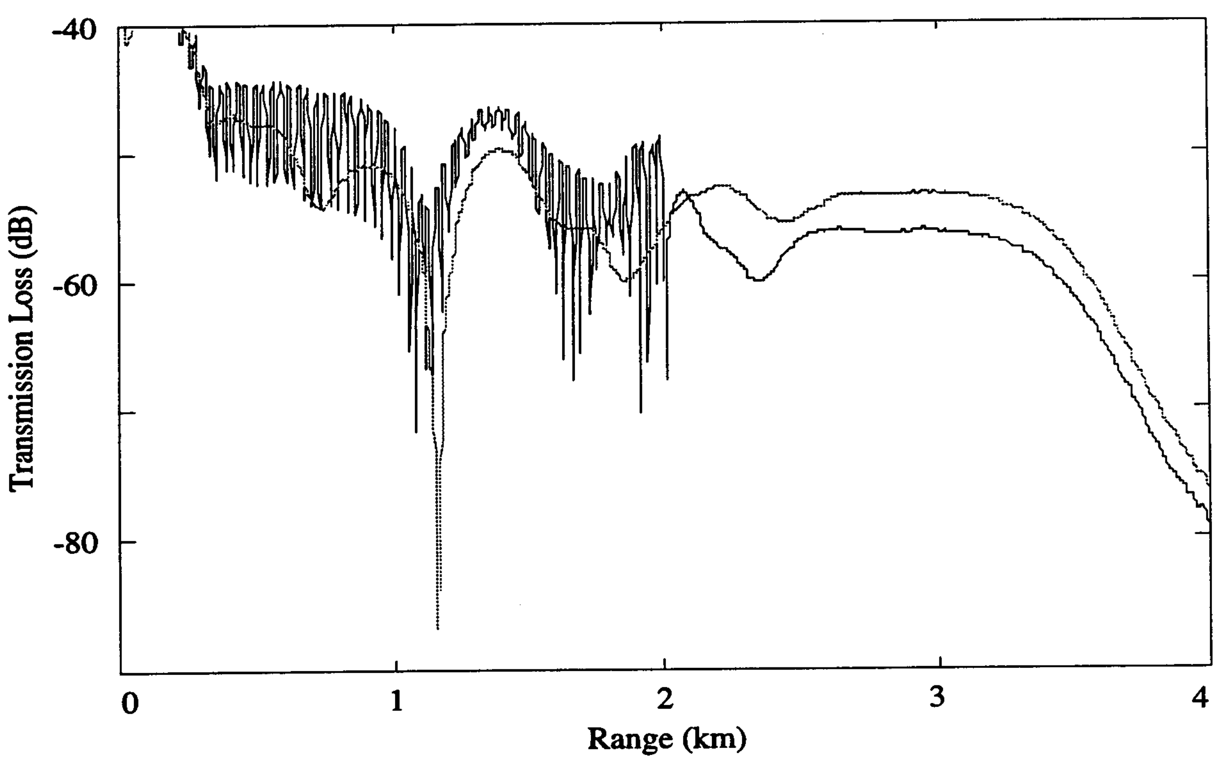

Fig. 6 — TL in environment from Fig. 5 overlaid on TL curve from unmodified wedge problem from Fig. 4a.

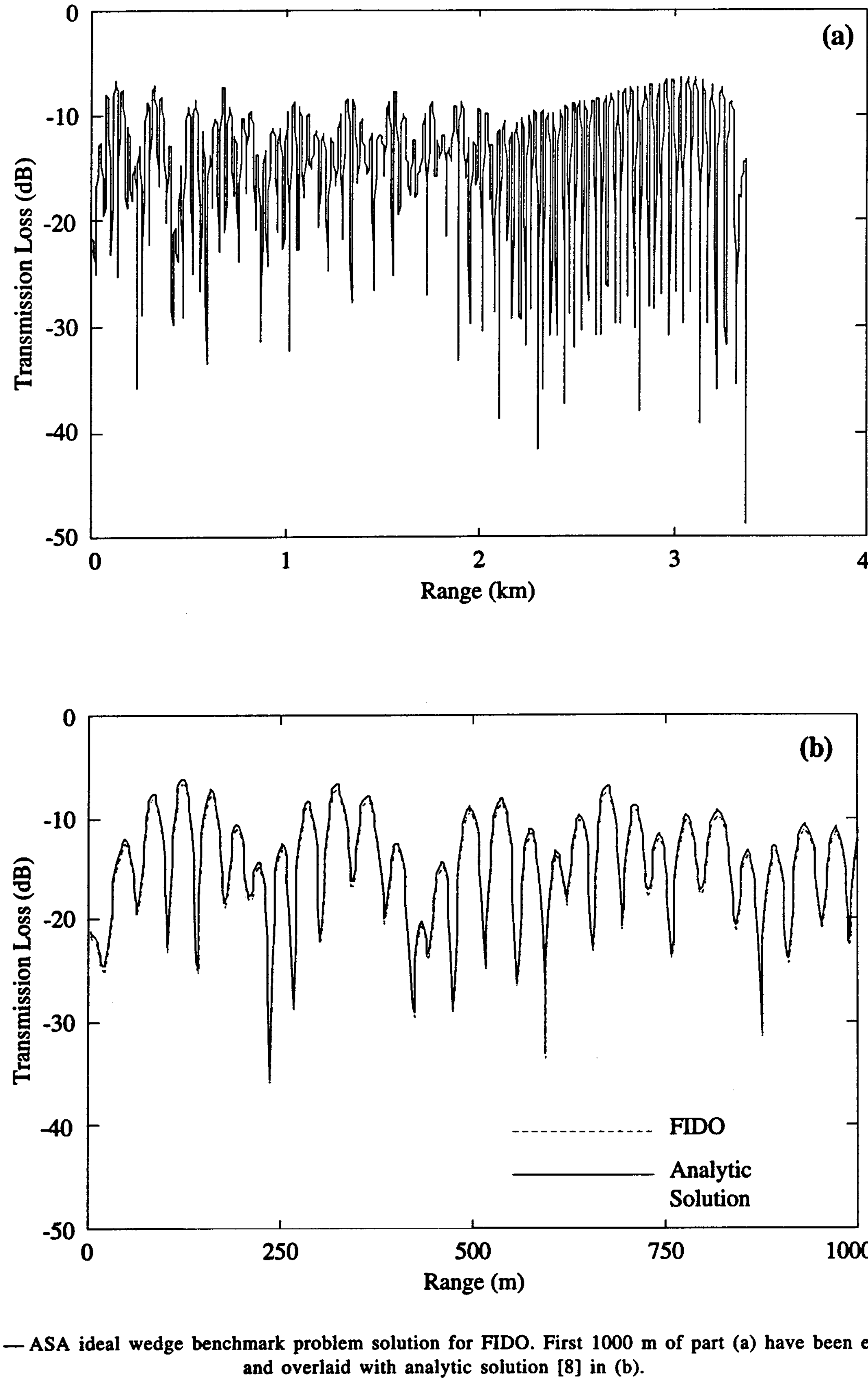

Fig. 7 — ASA ideal wedge benchmark problem solution for FIDO. First 1000 m of part (a) have been expanded and overlaid with analytic solution [8] in (b).

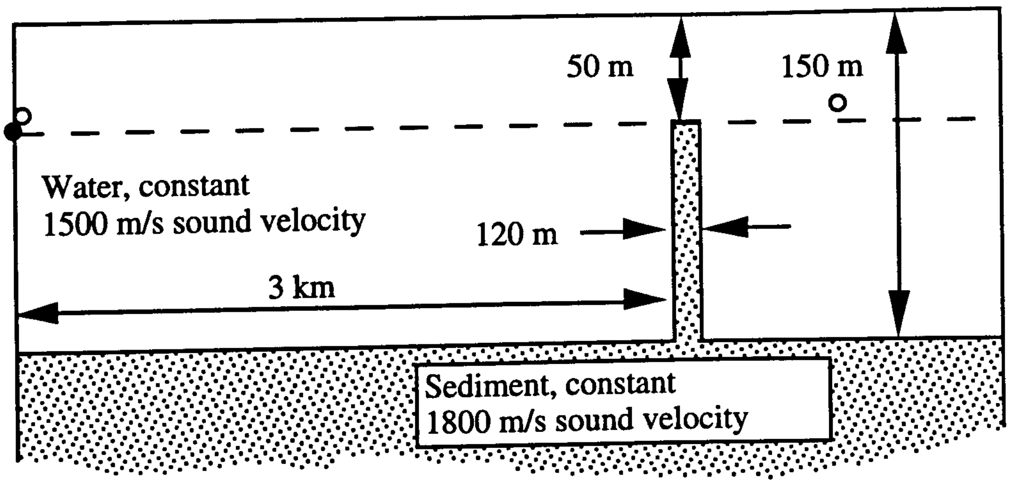

Fig. 8 — Reverberation and Scattering Workshop Test Case 2a environment. Source depth is 50 m (filled circle); receivers are located 45 m deep at 5- and 3500-m range (hollow circles). The thickness of the obstacle at 3000-m range is 2 wavelengths of the 30-Hz center frequency.

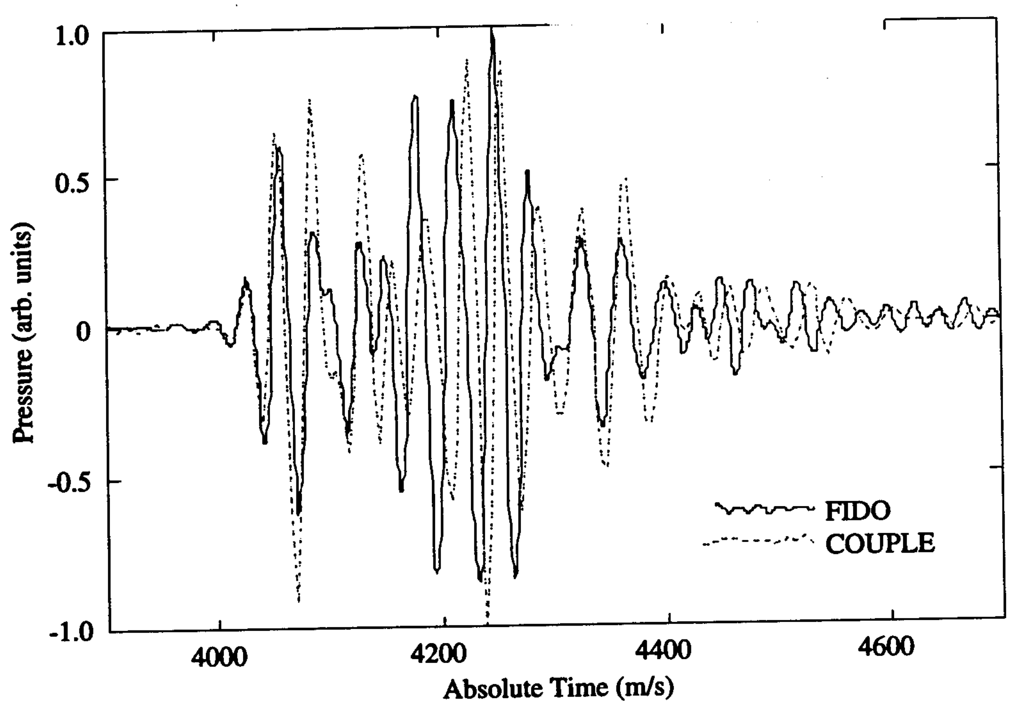

Fig. 9 — TS from FIDO and COUPLE calculations for backscattered pulse at near-source receiver in environment shown in Fig. 8. Solutions are identical for the first two cycles, after which discrepancies arise due to different treatments of attenuation.

SUMMARY AND CONCLUSIONS

The computer code FIDO provides another means of solving the underwater acoustic wave equation in complicated, realistic environments. It is of particular value because it uses a direct approach to this problem, which is seldom implemented, yet it requires no more computation time on modern vector and parallel computers than more commonly used indirect methods. The propagation, scattering, and absorption portions of FIDO combine to give solutions that agree with those of analytic solutions and standard reference models for the ASA range-dependent benchmarks, as well as for other problems.

ACKNOWLEDGMENTS

This work was supported by the Office of Naval Research (ONR-T) under Program Element 0602435N, Dr. W. Moseley, Program Manager, and by the Naval Research Laboratory Connection Machine Facility.

REFERENCES

1. R. A. Stephen, "Solutions to Range-Dependent Benchmark Problems," *J. Acoust. Soc. Am.* **87**, 1527–1534 (1990).

2. S. K. Numritch, R. A. Krutar, and R. Squier, "Computation of Acoustic Fields on a Massively Parallel Processor Using Lattice Gas Methods," in *Proceedings of the 3rd IMACS Symposium on Computational Acoustics, Vol. 1,* R. L. Lau, D. Lee, and A. R. Robinson, eds. (North-Holland, 1993).

3. F. Jensen and C. M. Ferla, "Numerical Solutions of Range-Dependent Benchmark Problems in Ocean Acoustics," *J. Acoust. Soc. Am.* **87**, 1499–1510 (1990).

4. R. A. Zingarelli, "Parabolic Equation Codes: Supercomputer vs. Workstation Performance Benchmarks," Naval Research Laboratory, SSC, MS, NRL Memorandum Report NRL/MR/7181--93-7015 (1993).

5. M. D. Collins, "FEPE User's Guide," Naval Research Laboratory, SSC, MS, NORDA Technical Note 365 (1988).

6. R. B. Evans, "A Coupled Mode Solution for Acoustic Propagation in a Waveguide with Stepwise Depth Variations of a Penetrable Bottom," *J. Acoust. Soc. Am.* **74**, 188–195 (1983).

7. M. J. Buckingham and A. Tolstoy, "An Analytical Solution for the Benchmark Problem 1: The Ideal Wedge," *J. Acoust. Soc. Am.* **87**, 1511-1513 (1990).

8. *Proceedings of the Reverberation and Scattering Workshop,* S. A. Chin-Bing, D. B. King, J. A. Davis, and R. B. Evans, eds. (in press).